J|A|C|S ARTICLES

Published on Web 08/13/2010

Effects of Oxygen Content on $Bi_3Mn_3O_{11+\delta}$: From 45 K Antiferromagnetism to Room-Temperature True Ferromagnetism

Alexei A. Belik* and Eiji Takayama-Muromachi

International Center for Materials Nanoarchitectonics, National Institute for Materials Science, 1-1 Namiki, Tsukuba, Ibaraki 305-0044, Japan

Received May 19, 2010; E-mail: alexei.belik@nims.go.jp

Abstract: The effects of oxygen content on the structural, physical, and chemical properties of $Bi_3Mn_3O_{11}$ with $KSbO_3$-type structure have been investigated. It was found that the oxygen content in $Bi_3Mn_3O_{11+\delta}$ can vary over a wide δ range, keeping the same cubic structure (space group $Pn\bar{3}$, $a = 9.12172(5)$ Å for $\delta = -0.5$, $a = 9.13784(8)$ Å for $\delta = 0$, and $a = 9.09863(7)$ Å for $\delta = 0.6$) and semiconducting properties of the material. At the same time, magnetic properties change from true antiferromagnetic with $T_N = 45$ K for $\delta = -0.5$ to true ferromagnetic with $T_C = 307$ K for $\delta = +0.6$. $Bi_3Mn_3O_{11}$ ($\delta = 0$) shows ferrimagnetic-like properties with $T_C = 150$ K and features typical for a re-entrant spin-glass below 30 K. Noticeable changes of the magnetic transition temperature and magnetism in $Bi_3Mn_3O_{11+\delta}$ with δ can be compared with changes of the magnetic and electronic properties of $LaMnO_{3+\delta}$, $BiMnO_{3+\delta}$, high-temperature copper superconductors (e.g., $YBa_2Cu_3O_{7+\delta}$), and other cuprates. $Bi_3Mn_3O_{11.6}$ shows a new record high T_C among insulating/semiconducting true ferromagnets. Our results demonstrate that the oxygen content can vary for the same cation composition in $KSbO_3$-type materials, and the oxygen content can be increased up to $BiMnO_{3.867}$ ($Bi_3Mn_3O_{11.6}$).

1. Introduction

ABO_3 compounds crystallize in a number of structure types, including perovskite, pyroxene, corundum, ilmenite (ordered corundum), hexagonal manganites, bixbyite, rare earth sesquioxide structures, $PbReO_3$, $KSbO_3$, $AlFeO_3$, and others.[1] The $KSbO_3$-type family (space group $Pn\bar{3}$) has only about a dozen of representatives, e.g., $KSbO_3$, $KIrO_3$,[2] $Bi_3GaSb_2O_{11}$,[3,4] $Bi_3AlSb_2O_{11}$,[4] $Bi_2NaSb_3O_{11}$,[5] $Bi_3M_3O_{11}$ (M = Ru,[6−8] Re,[9] Os[8]), $La_3Ru_3O_{11}$,[10−12] and $Pb_6Re_6O_{19}$.[13] Nevertheless, this class of materials is quite interesting because the oxygen content changes from ABO_3 to $ABO_{3.667}$. The $KSbO_3$-type structure is built from the corner- and edge-shared SbO_6 octahedra forming a three-dimensional framework with channels.[3] The channels are filled with K^+ ions in $KSbO_3$ ($K \cdot SbO_3$) and with Bi_3O_2 units in $Bi_3Ru_3O_{11}$ ($Bi_3O_2 \cdot 3RuO_3$) in an ordered manner. Disordered filling of the channels by K^+ ions in $KBiO_3$,[14] Na^+ ions in $NaSbO_3$,[15] and Sr^{2+} ions in $Sr_2Re_3O_9$[9] resulted in space group $Im\bar{3}$. The channels can also be filled by other units, e.g. La_4O, forming $La_4Ru_6O_{19}$ ($La_4O \cdot 6RuO_3$) and related compounds $La_4M_6O_{19}$[9] that deviate from the A:B = 1:1 stoichiometry and have a different space group of $I23$.[11,12] Variations in the oxygen content for the same cation composition have not been reported for the $KSbO_3$-type materials, even though some of them have 4d and 5d transition metals with variable oxidation states. The oxygen content is known to have crucial and dramatic effects on the properties of materials, e.g., on magnetic and electronic properties of high-temperature copper superconductors (e.g., $YBa_2Cu_3O_{7+\delta}$)[16] or perovskites (e.g., $LaMnO_{3+\delta}$,[17,18] $BiMnO_{3+\delta}$,[19−21]

(1) Giaquinta, D. M.; zur Loye, H.-C. *Chem. Mater.* **1994**, *6*, 365.
(2) Hoppe, R.; Claes, K. *J. Less-Common Metals* **1975**, *43*, 129.
(3) Sleight, W.; Bouchard, R. J. *Inorg. Chem.* **1973**, *12*, 2314.
(4) (a) Ismunandar; Kennedy, B. J.; Hunter, B. A. *Solid State Commun.* **1998**, *108*, 649. (b) Ismunandar; Kennedy, B. J.; Hunter, B. A. *J. Solid State Chem.* **1996**, *127*, 178.
(5) Champarnaud-Mesjard, J. C.; Frit, B.; Aftati, A.; El Farissi, M. *Eur. J. Solid State Inorg. Chem.* **1995**, *32*, 495.
(6) (a) Facer, G. R.; Elcombe, M. M.; Kennedy, B. J. *Aust. J. Chem.* **1993**, *46*, 1897. (b) Abraham, F.; Thomas, D. *Bull. Soc. Chim. Fr.* **1975**, 25.
(7) Tsuchida, K.; Kato, C.; Fujita, T.; Kobayashi, Y.; Sato, M. *J. Phys. Soc. Jpn.* **2004**, *73*, 698.
(8) Fujita, T.; Tsuchida, K.; Yasui, Y.; Kobayashi, Y.; Sato, M. *Physica B* **2003**, *329*, 743.
(9) Suzuki, H.; Ozawa, H.; Sato, H. *J. Phys. Soc. Jpn.* **2007**, *76*, 044805.
(10) (a) Cotton, F. A.; Rice, C. E. *J. Solid State Chem.* **1978**, *25*, 137. (b) Abraham, F.; Trehoux, J.; Thomas, D. *Mater. Res. Bull.* **1978**, *13*, 805.
(11) Khalifah, P.; Nelson, K. D.; Jin, R.; Mao, Z. Q.; Liu, Y.; Huang, Q.; Gao, X. P. A.; Ramirez, A. P.; Cava, R. J. *Nature* **2001**, *411*, 669.
(12) Khalifah, P.; Cava, R. J. *Phys. Rev. B* **2001**, *64*, 085111.
(13) Abakumov, A. M.; Shpanchenko, R. V.; Antipov, E. V. *Z. Anorg. Allg. Chem.* **1998**, *624*, 750.
(14) Nguyen, T. N.; Giaquinta, D. M.; Davis, W. M.; zur Loye, H. C. *Chem. Mater.* **1993**, *5*, 1273.
(15) Hong, H. Y.-P.; Kafalas, J. A.; Goodenough, J. B. *J. Solid State Chem.* **1974**, *9*, 345.
(16) Strobel, P.; Capponi, J. J.; Chaillout, C.; Marezio, M.; Tholence, J. L. *Nature* **1987**, *327*, 306.
(17) Topfer, J.; Goodenough, J. B. *J. Solid State Chem.* **1997**, *130*, 117.
(18) Maurin, I.; Barboux, P.; Lassailly, Y.; Boilot, J. P.; Villain, F.; Dordor, P. *J. Solid State Chem.* **2001**, *160*, 123.
(19) Sundaresan, A.; Mangalam, R. V. K.; Iyo, A.; Tanaka, Y.; Rao, C. N. R. *J. Mater. Chem.* **2008**, *18*, 2191.
(20) Belik, A. A.; Kolodiazhnyi, T.; Kosuda, K.; Takayama-Muromachi, E. *J. Mater. Chem.* **2009**, *19*, 1593.
(21) Belik, A. A.; Kodama, K.; Igawa, N.; Shamoto, S.; Kosuda, K.; Takayama-Muromachi, E. *J. Am. Chem. Soc.* **2010**, *132*, 8137.

10.1021/ja1043598

and $(BiMn_3)Mn_4O_{12}$).[22] In $LaMnO_{3+\delta}$,[17,18] the change in δ results in changes from an antiferromagnetic insulator to a ferromagnetic insulator to a ferromagnetic metal; at the same time, crystal symmetries are also changed.

Recently, we have succeeded in preparing the first example of a $KSbO_3$-type material containing a 3d transition metal, namely, $Bi_3Mn_3O_{11}$.[23] $Bi_3Mn_3O_{11}$ shows quite interesting magnetic properties: a ferrimagnetic-like transition near 150 K with features typical for re-entrant spin-glass below 30 K. We have also demonstrated the possibility of forming oxygen-deficient $Bi_3Mn_3O_{11-\delta}$ samples by heating $Bi_3Mn_3O_{11}$.[23] The properties of $Bi_3Mn_3O_{11-\delta}$ and $Bi_3Mn_3O_{11+\delta}$ have not been determined yet.

In this work, we demonstrate for the first time that the oxygen content of the $KSbO_3$-type materials can be increased further up to $ABO_{3.867}$ in $Bi_3Mn_3O_{11.6}$ ($Bi_3O_{2.6}\cdot 3MnO_3$), meaning that there is additional space in the channels of the structure. We also show that the oxygen content can vary for the same cation composition in $KSbO_3$-type materials. A wide variation of δ in $Bi_3Mn_3O_{11\pm\delta}$ keeps the same cubic structure and semiconducting properties of the material, compared, for example, with perovskites. At the same time, magnetic properties change from antiferromagnetic with $T_N = 45$ K for $\delta = -0.5$ to true ferromagnetic with $T_C = 307$ K for $\delta = +0.6$. $Bi_3Mn_3O_{11.6}$ shows a new record high ferromagnetic Curie temperature (T_C) among insulating/semiconducting true ferromagnets.[24]

2. Experimental Section

2.1. Synthesis and Determination of the Composition. $Bi_3Mn_3O_{11}$ was prepared from stoichiometric mixtures of Bi_2O_3 (99.9999%, Rare Metallic Co. Ltd.), MnO_2 (99.997%, Alfa Aesar), and $Bi_2O_{4.20}$ (99%, High Purity Chemicals Ltd.) according to the following reaction:[23]

$$13/12\,Bi_2O_3 + 3\,MnO_2 + 5/12\,Bi_2O_{4.20} \rightarrow Bi_3Mn_3O_{11} \quad (1)$$

The phase purity and oxygen content of MnO_2 were confirmed by X-ray powder diffraction (XRD) and thermogravimetric analysis (TGA). MnO_2 was the well-crystallized single-phase α modification. MnO_2 was heated in air to 923 K over 5 h and soaked there for 24 h (the experiment was performed in a conventional muffle furnace; the sample weights were measured before and after annealing). The final product was well-crystallized single-phase Mn_2O_3. The oxygen content calculated from the weight loss corresponded to $MnO_{2.01(1)}$. The oxygen content of a commercial Bi_2O_5 was found to be $Bi_2O_{4.20(2)}$ by TGA. The commercial Bi_2O_5 was heated in an SII Exstar 6000 (TG-DTA 6200) system to 770 K (10 K/min, Pt holder) in air, and the weight loss gave the composition of $Bi_2O_{4.20(2)}$. The final product after the TGA heat treatment was well-crystallized single-phase Bi_2O_3.

The synthesis of $Bi_3Mn_3O_{11}$ according to reaction 1 was performed in a belt-type high-pressure apparatus at 6 GPa and 1600 K for 40 min in Pt capsules.[23] After heat treatment, the samples were quenched to room temperature, and the pressure was slowly released. The resultant samples were dense black pellets. No noticeable change in the weight of the Pt capsules was found after the synthesis, indicating that the target oxygen content did not change during the reaction.

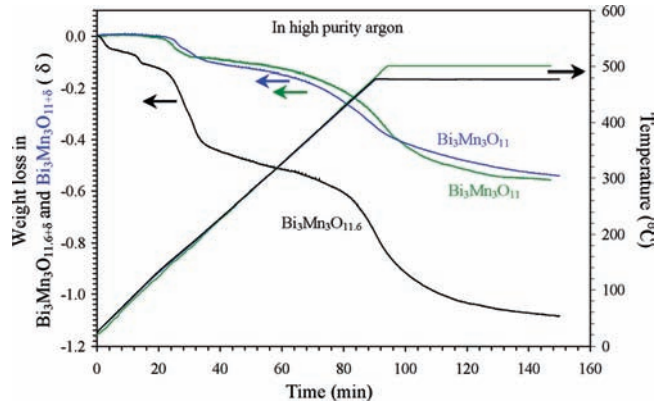

Figure 1. Thermogravimetric curves of $Bi_3Mn_3O_{11}$ (two different samples, blue and green curves) and $Bi_3Mn_3O_{11.6}$ (black curve) in high-purity Ar at a heating rate of 5 K/min. Note that the weight loss is given in δ for $Bi_3Mn_3O_{11+\delta}$ and $Bi_3Mn_3O_{11.6+\delta}$.

$Bi_3Mn_3O_{11.6}$ was prepared using the same synthesis conditions from stoichiometric mixtures of Bi_2O_3, MnO_2, and $Bi_2O_{4.20}$, taken for the target composition of $Bi_3Mn_3O_{12}$ according to the following reaction:

$$0.25\,Bi_2O_3 + 3\,MnO_2 + 1.25\,Bi_2O_{4.20} \rightarrow Bi_3Mn_3O_{11.6} + 0.2\,O_2 \quad (2)$$

The weight of Pt capsules after the synthesis changed noticeably, indicating that the Pt capsules were not able to maintain the generated oxygen pressure, and some oxygen escaped from the Pt capsules.

The oxygen content of the final products was determined by TGA in a mixture of 3% H_2 + 97% Ar using a Perkin-Elmer Pyris 1 TGA system in Al_2O_3 holders (the samples were heated to 873 K at a heating rate of 5 K/min and soaked there for 1 h). The samples decomposed to mixtures of Bi and MnO. The calculated oxygen content was $Bi_3Mn_3O_{11.00(1)}$ and $Bi_3Mn_3O_{11.60(1)}$ (see the Supporting Information). We note that the oxygen content determination by TGA or other chemical methods is based on certain assumptions, as discussed in ref 20. If some assumptions are not kept, a systematic shift may result. For example, the presence of impurities will affect the results of both TGA and (iodometric) titration techniques.

The $Bi_3Mn_3O_{10.5}$ sample (used for the property measurements) was prepared from $Bi_3Mn_3O_{11.60}$. $Bi_3Mn_3O_{11.60}$ was heated to 750 K and cooled to room temperature inside an oven in a magnetometer (Quantum Design MPMS). The average heating/cooling rate was about 1.5 K/min. Inside the oven, vacuum conditions were kept (about 1.3 kPa). $Bi_3Mn_3O_{\sim 10.5}$ can also be prepared from $Bi_3Mn_3O_{11.0}$ and $Bi_3Mn_3O_{11.6}$ by heating to 750−770 K in high-purity Ar (at a heating rate of 5 K/min and soaking time of 1 h) (Figure 1).

The cation ratio of $Bi_3Mn_3O_{11}$ and $BiMnO_3$ (used for comparison) was determined by electron probe microanalysis (EPMA) using a JEOL JXA-8500F instrument. The surface was polished on a fine alumina (1 μm)-coated film before the EPMA measurements. MnO and $Bi_4Ge_3O_{12}$ were used as standard materials for Mn and Bi. The Mn:Bi ratio determined by EPMA was 1.05(2) in $Bi_3Mn_3O_{11}$ and 1.05(6) in $BiMnO_3$.

2.2. Physical Properties. XRD data were collected at room temperature on a RIGAKU Ultima III diffractometer using Cu Kα radiation (2θ range of 10−120°, step width of 0.02°, and counting time of 10 s/step). Synchrotron XRD data for $Bi_3Mn_3O_{10.50}$ and $Bi_3Mn_3O_{11.60}$ were collected at room temperature using a large

(22) (a) Imamura, N.; Karppinen, M.; Motohashi, T.; Fu, D.; Itoh, M.; Yamauchi, H. *J. Am. Chem. Soc.* **2008**, *130*, 14948. (b) Imamura, N.; Karppinen, M.; Yamauchi, H. *Chem. Mater.* **2009**, *21*, 2179.
(23) Belik, A. A.; Takayama-Muromachi, E. *J. Am. Chem. Soc.* **2009**, *131*, 9504.
(24) Rogado, N. S.; Li, J.; Sleight, A. W.; Subramanian, M. A. *Adv. Mater.* **2005**, *17*, 2225.

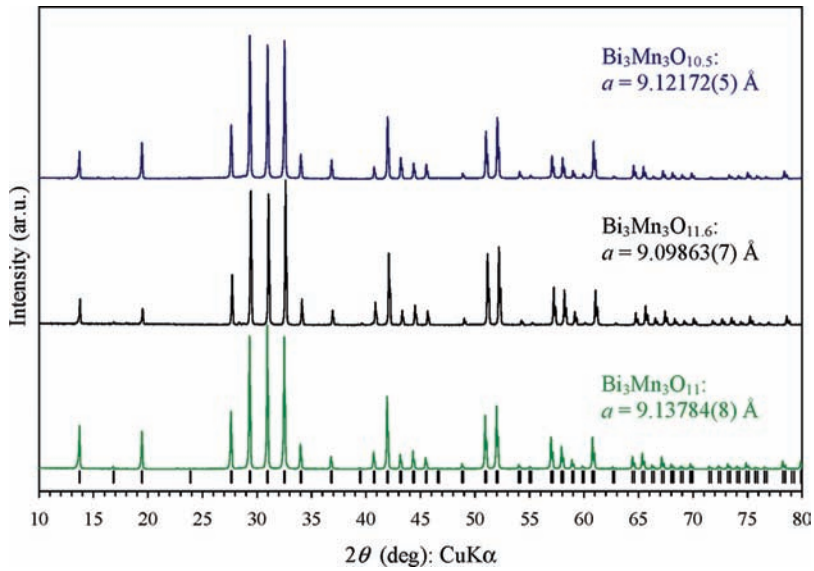

Figure 2. X-ray powder diffraction patterns (measured with Cu Kα radiation at room temperature) of $Bi_3Mn_3O_{10.5}$, $Bi_3Mn_3O_{11.6}$, and $Bi_3Mn_3O_{11}$. The refined lattice parameters are given. Possible Bragg reflections (space group $Pn\bar{3}$) are indicated by tic marks for $Bi_3Mn_3O_{11}$.

Debye−Scherrer camera at the BL02B2 beamline[25] of SPring-8. The incident beam from a bending magnet was monochromatized to $\lambda = 0.41916$ Å. The samples were contained in (boro)glass capillary tubes with an inner diameter of 0.2 mm, and the capillary tubes were rotated during measurements. The synchrotron XRD data were collected in a 2θ range from 1° to 75° with a step interval of 0.01° (the data from 2.5° to 52.5° were used in the refinements). Laboratory XRD and synchrotron XRD data were analyzed by the Rietveld method with RIETAN-2000 software.[26] High-temperature synchrotron XRD data of $Bi_3Mn_3O_{11}$ were collected at the BL02B2 beamline with $\lambda = 0.77412$ Å.

Magnetic susceptibilities, $\chi = \mathbf{M}/\mathbf{H}$, of $Bi_3Mn_3O_{11\pm\delta}$ were measured on a SQUID magnetometer (Quantum Design, MPMS) between 2 and 400 K in applied fields of 100 Oe, 1 kOe, and 10 kOe under both zero-field-cooled (ZFC) and field-cooled (FC; on cooling) conditions. The measurements between 300 and 750 K were performed using an oven attachment on heating and cooling at 10 kOe. Isothermal magnetization measurements were performed at 5, 100, 200, 300, and 350 K between −50 and 50 kOe and between 270 and 350 K with a step of 2 K from 50 to 0 kOe for $Bi_3Mn_3O_{11.6}$. T_C and T_N were roughly defined by the peak positions on the 100 Oe $d\chi/dT$ vs T and $d(\chi T)/dT$ vs T curves, respectively.

The specific heat, C_p, at magnetic fields of 0 and 70 kOe was recorded between 2 and 300 K (using an N Apiezon grease to make good thermal contacts between sample and holder) and between 250 and 400 K (using an H Apiezon grease) on cooling by a pulse relaxation method using a commercial calorimeter (Quantum Design PPMS).

Direct current (dc) electrical resistivity was measured between 10 and 400 K by the conventional four-probe method using a Quantum Design PPMS with the dc-gage current of 2 mA. The dc-gage current was reduced automatically at low temperatures to allow the resistivity measurements. Resistivity became too high to be measured with our system below 300 K for $Bi_3Mn_3O_{10.5}$, 130 K for $Bi_3Mn_3O_{11}$, and 180 K for $Bi_3Mn_3O_{11.6}$. At 300 K, $Bi_3Mn_3O_{11.6}$ showed an almost linear increase of resistivity as a function of magnetic field, reaching about a 15% increase at 90 kOe (see the Supporting Information). Pellets with approximate sizes of $5 \times 2 \times 1$ mm^3 were used for the measurements. Dielectric measurements of $Bi_3Mn_3O_{10.5}$ were performed between 5 and 300 K in the frequency range from 100 Hz to 1 MHz; no anomalies were detected near T_N (see the Supporting Information).

3. Results

3.1. X-ray Powder Diffraction of $Bi_3Mn_3O_{10.5}$, $Bi_3Mn_3O_{11}$, and $Bi_3Mn_3O_{11.6}$. Figure 2 depicts XRD patterns of $Bi_3Mn_3O_{10.5}$, $Bi_3Mn_3O_{11}$, and $Bi_3Mn_3O_{11.6}$. All the samples were almost single-phase with traces of unidentified impurities. $Bi_3Mn_3O_{11\pm\delta}$ crystallize in the $KSbO_3$-type structure (space group $Pn\bar{3}$) with $a = 9.12172(5)$ Å ($\delta = -0.5$), 9.13784(8) Å ($\delta = 0$), and 9.09863(7) Å ($\delta = 0.6$). A non-monotonic change of the lattice parameter with δ is probably the combination of different effects: contraction of the unit cell due to the increased amount of Mn^{5+} and expansion of the unit cell due to the increased number of oxygen ions in the channels. A non-monotonic change of the lattice parameter was also observed during *in situ* high-temperature synchrotron XRD measurements,[23] where the a parameter first jumps in $Bi_3Mn_3O_{10.9}$ compared with $Bi_3Mn_3O_{11}$ and then drops in $Bi_3Mn_3O_{10.5}$ (see also the Supporting Information).

3.2. Crystal Structure Analysis of $Bi_3Mn_3O_{10.5}$ and $Bi_3Mn_3O_{11.6}$. Fractional coordinates of $Bi_3Mn_3O_{11}$[23] were used as initial ones in the crystal structure analysis of $Bi_3Mn_3O_{10.5}$ and $Bi_3Mn_3O_{11.6}$. Fractional coordinates of the Bi1 site in $Bi_3Mn_3O_{11.6}$ were refined using a constraint $z = y$ (similar to $Bi_3Mn_3O_{11}$),[23] even though the Bi1 site is located in a general position (x,y,z). This constraint was used because the y and z coordinates were the same within standard deviations, and estimated standard deviations of y and z were about 1 order of magnitude larger when the y and z coordinates were refined independently. On the other hand, the x, y, and z coordinates of the Bi1 site could be refined in $Bi_3Mn_3O_{10.5}$. Attempts to split the Bi2 atom from the 4b site to the 8e site were unsuccessful in $Bi_3Mn_3O_{11}$ and $Bi_3Mn_3O_{11.6}$ (the x coordinate was almost zero, and the estimated standard deviation was huge). On the other hand, the Bi2 site was successfully split in $Bi_3Mn_3O_{10.5}$. With an occupation factor (g) of 1 for the O1, O2, and O3 sites, the thermal parameters (B) were normal in $Bi_3Mn_3O_{11.6}$, while B(O1) converged to 8.5(6) Å^2 in $Bi_3Mn_3O_{10.5}$. This fact shows that the oxygen vacancies

(25) Nishibori, E.; Takata, M.; Kato, K.; Sakata, M.; Kubota, Y.; Aoyagi, S.; Kuroiwa, Y.; Yamakata, M.; Ikeda, N. *Nucl. Instrum. Methods Phys. Res. Sect. A* **2001**, *467−468*, 1045.
(26) Izumi, F.; Ikeda, T. *Mater. Sci. Forum* **2000**, *321−324*, 198.

Table 1. Structure Parameters of $Bi_3Mn_3O_{10.5}$ and $Bi_3Mn_3O_{11.6}$ at Room Temperature[a]

site	Wyckoff position	*g*	*x*	*y*	*z*	*B* (Å^2)
			$Bi_3Mn_3O_{10.5}$			
Bi1	24*h*	1/3	0.4164(3)	0.3879(6)	0.3736(5)	1.62(5)
Bi2	8*e*	1/2	0.0091(2)	= *x*	= *x*	0.84(3)
Mn	12*g*	1	0.4041(3)	0.75	0.25	0.30(4)
O1	8*e*	0.75	0.1456(8)	= *x*	= *x*	1.0(4)
O2	12*f*	1	0.6163(11)	0.25	0.25	0.9(2)
O3	24*h*	1	0.5841(8)	0.2500(7)	0.5435(11)	1.2(2)
			$Bi_3Mn_3O_{11.6}$			
Bi1	24*h*	1/3	0.4009(2)	0.38175(13)	= *y*	0.61(2)
Bi2	4*b*	1	0	0	0	0.730(11)
Mn	12*g*	1	0.4044(2)	0.75	0.25	0.46(3)
O1	8*e*	1	0.1455(4)	= *x*	= *x*	0.4(2)
O2	12*f*	1	0.6147(8)	0.25	0.25	0.67(14)
O3	24*h*	1	0.5908(6)	0.2445(5)	0.5403(8)	0.62(13)

[a] Space group is $Pn\bar{3}$ (No. 201) at origin choice 2, $Z = 4$. *g* is the occupation factor. $Bi_3Mn_3O_{10.5}$: $a = 9.11919(8)$ Å and $V = 758.348(11)$ Å^3, $R_{wp} = 4.46\%$, $R_p = 3.22\%$, $R_B = 6.99\%$, and $R_F = 7.95\%$. d(Mn−O2) = 1.860(6) Å × 2, d(Mn−O3) = 1.886(10) Å × 2, d(Mn−O3) = 1.976(10) Å × 2. $Bi_3Mn_3O_{11.6}$: $a = 9.11151(6)$ Å and $V = 756.434(9)$ Å^3, $R_{wp} = 3.44\%$, $R_p = 2.28\%$, $R_B = 1.96\%$, and $R_F = 1.81\%$. d(Mn−O2) = 1.871(4) Å × 2, d(Mn−O3) = 1.908(6) Å × 2, d(Mn−O3) = 1.912(7) Å × 2.

are located at the O1 site in $Bi_3Mn_3O_{10.5}$. The same result was obtained during the structural analysis of $Bi_3Mn_3O_{11}$ using *in situ* high-temperature synchrotron XRD data at 740 K, where the oxygen content was close to $Bi_3Mn_3O_{10.5}$ (see the Supporting Information of ref 23). Using synchrotron XRD data, we could not localize additional oxygen atoms in $Bi_3Mn_3O_{11.6}$. Final structural parameters, *R* indexes, and Mn−O bond lengths of $Bi_3Mn_3O_{10.5}$ and $Bi_3Mn_3O_{11.6}$ at room temperature are listed in Table 1. Figure 3 shows fragments of the crystal structure of $Bi_3Mn_3O_{10.5}$. The Supporting Information gives other bond lengths and observed, calculated, and difference synchrotron XRD patterns.

3.3. Magnetic Properties of $Bi_3Mn_3O_{10.5}$, $Bi_3Mn_3O_{11}$, and $Bi_3Mn_3O_{11.6}$. Figure 4 shows the inverse magnetic susceptibilities as a function of temperature (χ^{-1} vs T) for three samples and actually one of the preparation routes for $Bi_3Mn_3O_{10.5}$. The curves were fit by the simple Curie−Weiss equation ($\chi = \mu_{eff}^2/[8(T-\theta)]$) between 400 and 550 K. The effective magnetic moment (μ_{eff}) per formula unit (f.u.) and the Curie−Weiss temperature (θ) were calculated as follows: $\mu_{eff} = 5.84\ \mu_B$ and $\theta = +217$ K in $Bi_3Mn_3O_{11}$ (the expected magnetic moment, μ_{exp}, is 6.16 μ_B); $\mu_{eff} = 5.37\ \mu_B$ and $\theta = +337$ K in $Bi_3Mn_3O_{11.6}$ ($\mu_{exp} = 5.57\ \mu_B$); and $\mu_{eff} = 6.58\ \mu_B$ and $\theta = -80$ K in $Bi_3Mn_3O_{10.5}$ ($\mu_{exp} = 6.70\ \mu_B$). The changes in the experimental μ_{eff} values are in very good agreement with the changes of the oxidations states of Mn atoms ($Bi_3Mn^{4+}{}_3O_{10.5}$, $Bi_3Mn^{4+}{}_2Mn^{5+}O_{11}$, and, for simplicity, $Bi_3Mn^{4+}Mn^{5+}{}_2O_{11.5}$). This fact also shows that Mn ions are responsible for the charge compensation in $Bi_3Mn_3O_{11\pm\delta}$, not Bi ions. $Bi_3Mn_3O_{11.6}$ demonstrates clearly a ferromagnetic-like transition with $T_C = 310-315$ K (a temperature step during the magnetization measurements was 5 K in this temperature range), and it has a large positive Curie−Weiss temperature. (T_C will be estimated more precisely below.) $Bi_3Mn_3O_{10.5}$ shows clearly an antiferromagnetic transition with the Neel temperature, T_N, of 45 K, and it has a negative Curie−Weiss temperature. The ZFC and FC curves of $Bi_3Mn_3O_{11.6}$ were almost constant below about 250 K, without any additional anomalies at low temperatures (see the Supporting Information) compared with $Bi_3Mn_3O_{11}$, where features typical for a re-entrant spin-glass were observed below 30 K.[23] The

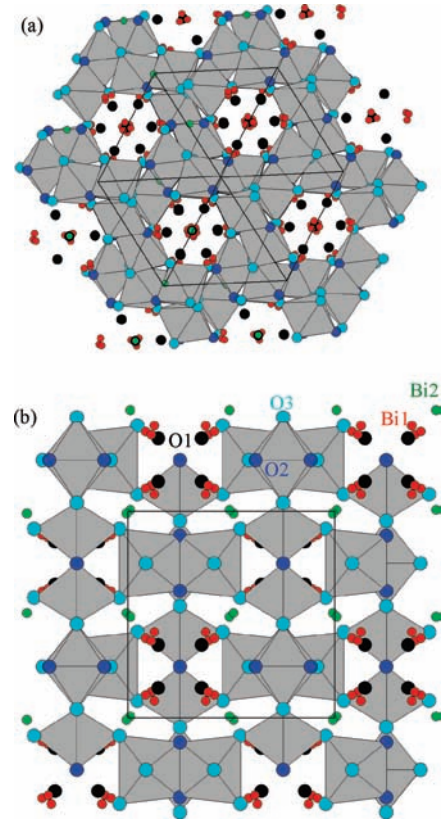

Figure 3. Fragments of the crystal structure of $Bi_3Mn_3O_{10.5}$ with the split Bi1 and Bi2 atoms. The MnO_6 octahedra are shown in gray. The O1 atoms in the channels are given by black circles. (a) The view along the channel (111) direction. (b) The view along the *a* axis.

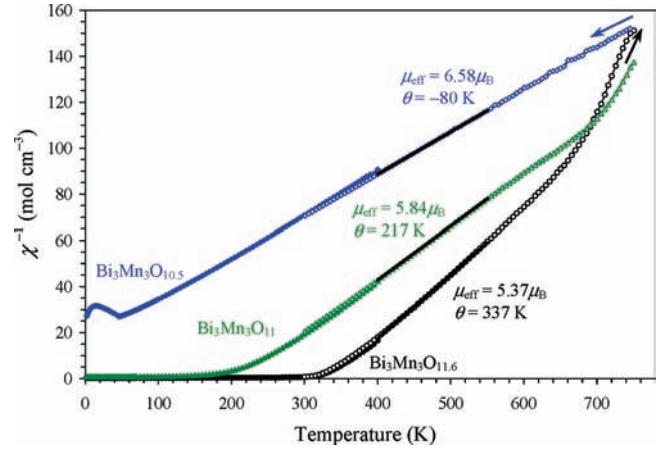

Figure 4. Inverse magnetic susceptibilities of $Bi_3Mn_3O_{10.5}$, $Bi_3Mn_3O_{11}$, and $Bi_3Mn_3O_{11.6}$. The measurements were performed at 10 kOe between 2 and 400 K (filled symbols) and between 300 and 750 K (open symbols) using an oven attachment. The linear curves between 400 and 550 K depict the Curie−Weiss fits, with the fitting parameters given in the figure. The arrows demonstrate the preparation route of $Bi_3Mn_3O_{10.5}$ from $Bi_3Mn_3O_{11.6}$ inside the oven during the measurements.

magnetic properties of $Bi_3Mn_3O_{11}$ are consistent with ferrimagnetic behavior.[23] $Bi_3Mn_3O_{11}$ is called a ferrimagnet because its saturated magnetization reaches only a portion (3.19 μ_B at 5 K and 50 kOe)[23] of the maximum value (8 μ_B), even though it has a positive Curie−Weiss temperature of 217 K. The Curie−Weiss temperature is actually a sum of different interactions between magnetic ions. In most cases, a positive Curie−Weiss temperature corresponds to ferromagnets, and a

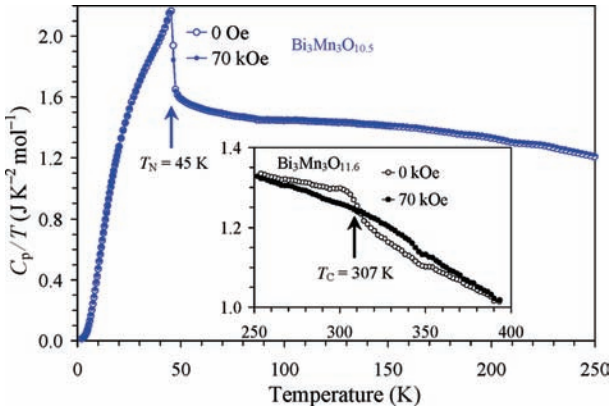

Figure 5. Specific heat data for $Bi_3Mn_3O_{10.5}$ and $Bi_3Mn_3O_{11.6}$ (inset) at 0 Oe (open symbols) and 70 kOe (filled symbols) plotted as C_p/T vs T. An anomaly near 350 K is due to a sample holder.

negative Curie−Weiss temperature corresponds to antiferromagnets. However, there are exceptions. For example, $LaMnO_3$ is a classical (canted) antiferromagnet. However, it has a positive Curie−Weiss temperature of 52 K because the intraplane ferromagnetic interactions are much stronger than the interplane antiferromagnetic interactions.[27] The positive Curie−Weiss temperature of $Bi_3Mn_3O_{11}$ reflects the fact that ferromagnetic-type interactions are dominant. It is also difficult to consider $Bi_3Mn_3O_{11}$ as a canted antiferromagnet because of its positive Curie−Weiss temperature and large saturated magnetization.

Figure 5 depicts specific heat data of $Bi_3Mn_3O_{10.5}$ and $Bi_3Mn_3O_{11.6}$. $Bi_3Mn_3O_{10.5}$ shows a strong anomaly near T_N, which is almost independent of a magnetic field. This behavior is typical for antiferromagnets, and the data unambiguously confirmed the onset of the long-range antiferromagnetic order in $Bi_3Mn_3O_{10.5}$. $Bi_3Mn_3O_{11.6}$ has a weak anomaly near T_C, and a magnetic field smears the transition to a high temperature region, which is typical for ferromagnets. The specific heat anomaly in $Bi_3Mn_3O_{11.6}$ confirms the onset of long-range ferromagnetic order. The magnitude of an anomaly near T_C or T_N (or the amount of the released entropy) depends on many factors. The higher the temperature, the weaker the magnetic anomalies because of an increased contribution from the lattice. Competition between different interactions or frustration and structural disorder also significantly suppress magnetic anomalies near T_C or T_N. The above reasons may be responsible for the weak magnetic anomaly at T_C in the specific heat of $Bi_3Mn_3O_{11.6}$. Very weak magnetic anomalies at T_C were also found in the specific heat of $LaMnO_{3+\delta}$.[28] We note that no specific heat anomalies were observed in $Bi_3Mn_3O_{11}$.[23]

Isothermal magnetization curves (**M** vs **H**) are shown in Figure 6. In $Bi_3Mn_3O_{11.6}$ at 50 kOe, the magnetization reaches 7.33 μ_B/f.u. at 5 K (the value being very close to the full magnetization) and 3.51 μ_B/f.u. at 300 K. These results show that $Bi_3Mn_3O_{11.6}$ is a true ferromagnet. $Bi_3Mn_3O_{11.6}$ behaves as a very soft ferromagnet with negligible remnant magnetization (0.08 μ_B/f.u. at 5 K) and coercive field similar to those of ferrimagnetic metal Sr_2FeMoO_6[29] and ferromagnetic semiconductor $BiMnO_3$.[30] $Bi_3Mn_3O_{11.6}$ is attached to permanent magnets

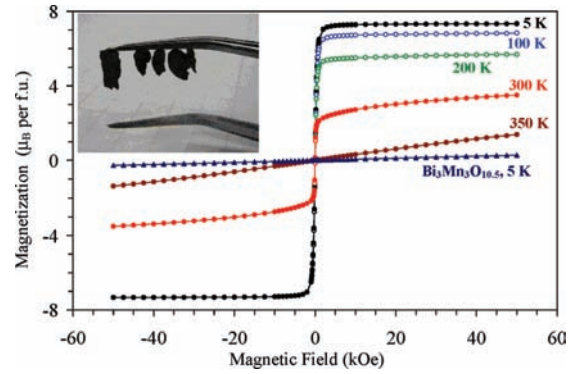

Figure 6. Isothermal magnetization curves for $Bi_3Mn_3O_{11.6}$ at 5, 100, 200, 300, and 350 K (circles) and for $Bi_3Mn_3O_{10.5}$ at 5 K (triangles). Inset shows pieces of $Bi_3Mn_3O_{11.6}$ attached to magnetized tweezers at room temperature.

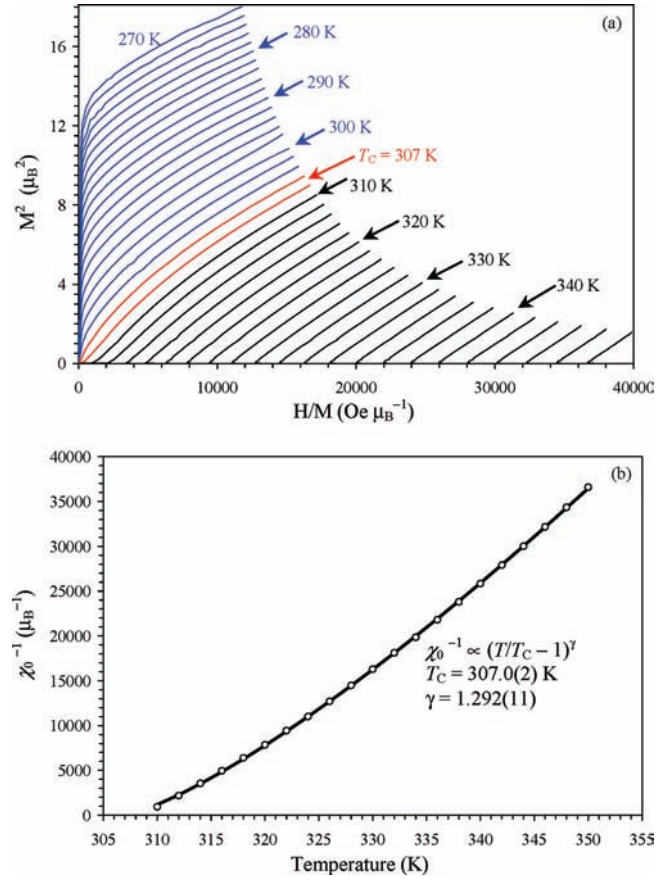

Figure 7. (a) Arrott plots ($\mathbf{M}^2$ vs $\mathbf{H}/\mathbf{M}$) for $Bi_3Mn_3O_{11.6}$ from 270 to 350 K with a step of 2 K. (b) Inverse initial susceptibilities (χ_0^{-1}; circles) versus temperature for $Bi_3Mn_3O_{11.6}$. The line shows the fitting results, with the equation and fitting parameters given in the figure.

and magnetized objects at room temperature (see the inset of Figure 6). At 350 K, an almost linear behavior was observed on the **M** vs **H** curves of $Bi_3Mn_3O_{11.6}$. In antiferromagnetic $Bi_3Mn_3O_{10.5}$, linear **M** vs **H** curves were found at 5 K without any signs of hysteretic behavior.

To estimate T_C of $Bi_3Mn_3O_{11.6}$ more precisely, we used the Arrott plots ($\mathbf{M}^2$ vs $\mathbf{H}/\mathbf{M}$; Figure 7a). The Arrott plots deviate from linear behavior near T_C, similar to some other ferromagnets.[31] Therefore, we estimated the inverse initial susceptibilities (χ_0^{-1}) by smooth extrapolation of the $\mathbf{M}^2$ vs $\mathbf{H}/\mathbf{M}$ curves above

(27) Zhou, J.-S.; Goodenough, J. B. *Phys. Rev. B* **1999**, *60*, 15002.
(28) Ghivelder, L.; Castillo, I. A.; Gusmao, M. A.; Alonso, J. A.; Cohen, L. F. *Phys. Rev. B* **1999**, *60*, 12184.
(29) Kobayashi, K. L.; Kimura, T.; Sawada, H.; Terakura, K.; Tokura, Y. *Nature* **1998**, *395*, 677.

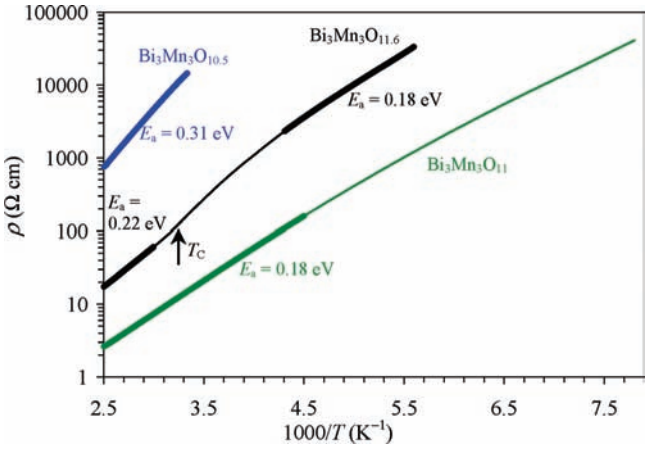

Figure 8. Direct current resistivity data for $Bi_3Mn_3O_{10.5}$, $Bi_3Mn_3O_{11}$, and $Bi_3Mn_3O_{11.6}$. The data are plotted as ρ (in logarithmic scale) vs $10^3/T$. The bold lines show temperature regions used for the estimation of the activation energy.

T_C on the H/M axis. The χ_0^{-1} vs T curve (Figure 7b) was fit by the simple equation,[31] $\chi_0^{-1} = A(T/T_C - 1)^{\gamma}$, with the parameters of $T_C = 307.0(2)$ K and $\gamma = 1.292(11)$.

3.4. Transport Properties of $Bi_3Mn_3O_{10.5}$, $Bi_3Mn_3O_{11}$, and $Bi_3Mn_3O_{11.6}$. Figure 8 demonstrates that $Bi_3Mn_3O_{10.5}$, $Bi_3Mn_3O_{11}$, and $Bi_3Mn_3O_{11.6}$ have semiconducting-type conductivity. The activation energies in $Bi_3Mn_3O_{11}$ (between 225 and 400 K) and $Bi_3Mn_3O_{11.6}$ (between 180 and 230 K) were almost the same (0.18 eV). This fact shows that these compounds behave as narrow-band semiconductors. $Bi_3Mn_3O_{11.6}$ shows a small change of the activation energy above T_C. The activation energy in $Bi_3Mn_3O_{10.5}$ was about 0.31 eV. $Bi_3Mn_3O_{11.6}$ should have additional oxygen atoms in the channel of the structure. Mobility of oxygen atoms at higher temperatures may be responsible for the change of the activation energy.

4. Discussion

Even though the target composition was $Bi_3Mn_3O_{12}$, the resultant sample had the composition of $Bi_3Mn_3O_{11.6}$. This fact shows that 11.6 is the maximum oxygen content at the synthesis conditions, and the structure cannot accommodate more oxygen. The TGA data in hydrogen (see the Supporting Information) and Ar (Figure 1) clearly confirmed that $Bi_3Mn_3O_{11.6}$ contains more oxygen than $Bi_3Mn_3O_{11}$. We note that $Bi_3Mn_3O_{10.5}$ could only be prepared from $Bi_3Mn_3O_{11}$ or $Bi_3Mn_3O_{11.6}$ by heating in an inert atmosphere or in a vacuum. The direct high-pressure high-temperature synthesis of $Bi_3Mn_3O_{10.5}$ produced a sample containing a lot of impurities (see the Supporting Information). We should also emphasize step-like weight changes in $Bi_3Mn_3O_{11}$ and $Bi_3Mn_3O_{11.6}$ on heating (Figure 1). This fact shows that other compositions with intermediate oxygen contents can be stabilized, for example, $Bi_3Mn_3O_{10.9}$.

Oxygen content has a drastic effect on the magnetism of $Bi_3Mn_3O_{11\pm\delta}$ and on the nature of magnetic interactions. $Bi_3Mn_3O_{10.5}$, with the transition metal in one oxidation state of 4+, has antiferromagnetic interactions between Mn^{4+} ions and a rather low T_N of 45 K. Note that $Bi_3Mn_3O_{10.5}$ behaves as a true antiferromagnet, that is, without any signs of spin canting. Introduction of Mn^{5+} ions into the system seems to produce ferromagnetic-type interactions and increase the strength of interactions and, therefore, transition temperatures. $Bi_3Mn_3O_{11}$, with one-third of Mn^{5+} ions, shows ferrimagnetic-like properties and a transition temperature of about 150 K.[23] The appearance of spin-glass properties below 30 K in $Bi_3Mn_3O_{11}$ gives support for strong competition between antiferromagnetic and ferromagnetic interactions. $Bi_3Mn_3O_{11.6}$, with about two-thirds of Mn^{5+}, shows room-temperature ferromagnetism. Noticeable changes of the magnetic transition temperature and magnetism in $Bi_3Mn_3O_{11+\delta}$ with δ can be compared with significant changes of the magnetic and electronic properties of perovskite-like $LaMnO_{3+\delta}$[17,18] and $BiMnO_{3+\delta}$,[19–21] high-temperature copper superconductors (e.g., $YBa_2Cu_3O_{7+\delta}$),[16] and other cuprates (e.g., $Sr_2Cu(Re_{0.69}Ca_{0.31})O_{6+\delta}$).[32] However, compared with perovskite-type materials and cuprates, $KSbO_3$-type materials have been investigated poorly, especially from the theoretical point of view.[12] In perovskites $LaMnO_{3+\delta}$[17,18] and $BiMnO_{3+\delta}$,[19–21] the crystal symmetry changes with changing δ, in comparison with $Bi_3Mn_3O_{11\pm\delta}$, where the cubic structure is stable over a wide δ range. The structural stability of $Bi_3Mn_3O_{11\pm\delta}$ can probably be explained by its channel-like feature (Figure 3): (additional) oxygen atoms should be located in the channels, and they are removed from the channels as confirmed by the structural analysis of $Bi_3Mn_3O_{10.5}$. The formula $Bi_3Mn_3O_{11\pm\delta}$ seems to reflect the real changes in the composition. In perovskites, cation vacancies $La_{1-x}Mn_{1-x}O_3$ are actually formed, even though the formula is written as $LaMnO_{3+\delta}$ for simplicity. Detailed structural investigations and localization of additional oxygen in $Bi_3Mn_3O_{11.6}$ are left for future work. Some structural differences among $Bi_3Mn_3O_{10.5}$, $Bi_3Mn_3O_{11}$, and $Bi_3Mn_3O_{11.6}$ can be seen from the available data. The formation of oxygen vacancies in the channels of the $Bi_3Mn_3O_{10.5}$ structure results in increased disordering of Bi atoms in the channels: the Bi1 atoms are split by about 0.5 Å in $Bi_3Mn_3O_{10.5}$, 0.35 Å in $Bi_3Mn_3O_{11}$, and 0.25 Å in $Bi_3Mn_3O_{11.6}$; the Bi2 atoms are split by about 0.3 Å in $Bi_3Mn_3O_{10.5}$ and show no splitting in $Bi_3Mn_3O_{11}$ and $Bi_3Mn_3O_{11.6}$. The increased disordering of Bi atoms can be explained by the fact that Bi atoms become underbonded with the formation of oxygen vacancies. We note that R_B and R_F indexes in $Bi_3Mn_3O_{10.5}$ were significantly larger that those of $Bi_3Mn_3O_{11}$[23] and $Bi_3Mn_3O_{11.6}$ (Table 1). This fact may indicate additional structural disorder, which cannot be represented by the split-atom model.

The origin of ferromagnetism in $LaMnO_3$-based materials has been investigated extensively using experimental and theoretical approaches (the parent compound $LaMnO_3$ is an antiferromagnetic insulator). The double-exchange mechanism between Mn^{3+} and Mn^{4+} is capable of describing many experimental data on these materials in the ferromagnetic metallic regime.[33] However, there exists a ferromagnetic semiconducting phase in $LaMnO_{3+\delta}$,[17,18] $La_{1-x}Ca_xMnO_3$,[33] and $La_{1-x}Sr_xMnO_3$ in very narrow δ and x ranges. For example, in $LaMnO_{3+\delta}$, semiconducting ferromagnetic phases with $T_C \approx 200$ K exist near $\delta \approx 0.10$. Some analogies can be seen in $Bi_3Mn_3O_{11\pm\delta}$: $Bi_3Mn_3O_{10.5}$ with Mn^{4+} ions is an antiferromagnet, and $Bi_3Mn_3O_{11.6}$ is a semiconducting ferromagnet containing Mn^{4+} and Mn^{5+} ions. If a metallic ferromagnetic phase exists in $Bi_3Mn_3O_{11+\delta}$, it should appear for $\delta > 0.6$, which could not be achieved in our experiments. Magnetic and transport properties of $LaMnO_3$-based materials strongly depend on Mn−O−Mn bond angles,

(30) Kimura, T.; Kawamoto, S.; Yamada, I.; Azuma, M.; Takano, M.; Tokura, Y. *Phys. Rev. B* **2003**, *67*, 180401.
(31) Kouvel, J. S.; Fisher, M. E. *Phys. Rev.* **1964**, *A136*, 1626.
(32) Isobe, M.; Kimoto, K.; Takayama-Muromachi, E. *J. Magn. Magn. Mater.* **2007**, *312*, 91.
(33) Edwards, D. M. *Adv. Phys.* **2002**, *51*, 1259.

which are 180° in the ideal perovskite structure with corner-shared MnO_6 octahedra. $Bi_3Mn_3O_{11}$ has a different framework made of edge- and corner-shared MnO_6 octahedra (Figure 3). The Mn−O−Mn bond angles are about 100° and 130° in $Bi_3Mn_3O_{11}$.[23] Therefore, it is difficult to apply classical rules with 90° or 180° cation−anion−cation bridges (e.g., Goodenough−Kanamori rules). It is interesting to note that $Bi_3Mn_3O_{11\pm\delta}$ maintains semiconducting properties, while similar compounds $Bi_3M_3O_{11}$ with 4d and 5d transition metals have been reported to have metallic-like conductivity.[7–9,11]

Materials possessing ferromagnetic properties at room temperature are of great practical interest.[34−38] They are used in magnetic data storage, transformer cores, permanent magnets, and so forth. Ferromagnetic dielectrics for spin polarization[34] and ferromagnetic diluted semiconductors[35,36] for spin electronics have recently attracted much attention. Ferromagnetic-like properties are observed in *true* ferromagnets (that is, where the main interaction between magnetic ions is ferromagnetic), in canted antiferromagnets or so-called weak ferromagnets, and in ferrimagnets (where the main interaction between magnetic ions is antiferromagnetic, and ferromagnetic-like properties appear due to spin canting or uncompensated magnetic sublattices).[38] *True* ferromagnets usually have metallic conductivity, for example, the elemental metals Fe (with magnetic transition temperature $T_C = 1043$ K), Ni ($T_C = 627$ K),[31] and Co ($T_C = 1388$ K)[38] and oxides CrO_2 ($T_C = 386$ K),[38] $SrRuO_3$ ($T_C = 160$ K),[39] $LaMnO_{3+\delta}$ ($\delta \approx 0.14$, $T_C \approx 200$ K),[17,18] $La_{1-x}Sr_xMnO_3$ ($x \approx 0.3-0.5$, $T_C \approx 350$ K),[33] and EuO (Eu-rich, $T_C = 69$ K).[38,40] Antiferromagnets (including canted antiferromagnets and ferrimagnets) are usually insulators or semiconductors. Insulating/semiconducting ferromagnets are always exceptions to the general rule and, therefore, of interest not only from the practical point of view but also from the viewpoint of the mechanism. Many ferrimagnets and canted antiferromagnets have high magnetic ordering temperatures well above room temperature, for example, magnetite Fe_3O_4 ($T_C = 858$ K),[38] known since ancient times, and perovskites Sr_2FeMoO_6 ($T_C \approx 450$ K),[29,37] $Sr_2Cu(Re_{0.69}Ca_{0.31})O_6$ ($T_C = 440$ K),[32] $BiCu_3Mn_4O_{12}$ ($T_C = 350$ K),[41] and $Sr_{1-x}Y_xCoO_{3+\delta}$ ($T_C = 335$ K).[42] However, insulating *true* ferromagnets with high T_C's are very rare. The typical values of T_C are 100 K in $BiMnO_3$,[30,43] ~200 K in $LaMnO_{3+\delta}$ ($\delta \approx 0.10$),[17,18] ~200 K in $La_{1-x}Sr_xMnO_3$ ($x \approx 0.1$),[33] 180 K in $K_2Cr_8O_{16}$,[44] and 33 K in $CrBr_3$.[38] Before now, the highest Curie temperature for ferromagnetic insulators/semiconductors was reported for La_2MnNiO_6 ($T_C \approx 280$ K).[24,45] $Bi_3Mn_3O_{11.6}$ shows a new record high T_C among insulating/semiconducting true ferromagnets. Insulating/semiconducting ferromagnets are highly attractive materials for spin electronics.[34,46]

In conclusion, we showed that the oxygen content in $Bi_3Mn_3O_{11+\delta}$ varies in a wide δ range, keeping the same cubic structure and semiconducting properties of the material. We demonstrated for the first time that the oxygen content can vary for the same cation composition in $KSbO_3$-type materials, and the oxygen content can be increased further up to $BiMnO_{3.867}$ ($Bi_3Mn_3O_{11.6}$), meaning that there is additional space in the channels of the structure. We also discovered *true* ferromagnetism in a semiconducting material, which is rather rare.[24,34,38] $Bi_3Mn_3O_{11.6}$ is a ferromagnet with the highest Curie temperature ($T_C = 307$ K) for this class of materials (ferromagnetic insulators/semiconductors). The Curie temperature of $Bi_3Mn_3O_{11.6}$ is above room temperature, and which makes it very important for practical applications.

Acknowledgment. This work was supported by World Premier International Research Center Initiative (WPI Initiative, MEXT, Japan), the NIMS Individual-Type Competitive Research Grant, and the Japan Society for the Promotion of Science (JSPS) through its "Funding Program for World-Leading Innovative R&D on Science and Technology" (FIRST) Program. We thank Mr. K. Kosuda of NIMS for electron probe microanalysis. The synchrotron radiation experiments were performed at the SPring-8 with the approval of the Japan Synchrotron Radiation Research Institute (Proposal Numbers 2009A1136 and 2010A1215). We thank Dr. J. Kim and Dr. N. Tsuji for their assistance at SPring-8.

Supporting Information Available: Details of magnetization, resistivity, laboratory and synchrotron XRD, TGA, and dielectric measurements and bond lengths (PDF); X-ray crystallographic data (CIF). This material is available free of charge via the Internet at http://pubs.acs.org.

JA1043598

(34) Moodera, J. S.; Santos, T. S.; Nagahama, T. *J. Phys.: Condens. Matter* **2007**, *19*, 165202.
(35) Matsumoto, Y.; Murakami, M.; Shono, T.; Hasegawa, T.; Fukumura, T.; Kawasaki, M.; Ahmet, P.; Chikyow, T.; Koshihara, S.; Koinuma, H. *Science* **2001**, *291*, 854.
(36) Macdonald, H.; Schiffer, P.; Samarth, N. *Nat. Mater.* **2005**, *4*, 195.
(37) Serrate, D.; De Teresa, J. M.; Ibarra, M. R. *J. Phys.: Condens. Matter* **2007**, *19*, 023201.
(38) Kittel, C. *Introduction to Solid State Physics*; Wiley: New York, 1996.
(39) Mahadevan, P.; Aryasetiawan, F.; Janotti, A.; Sasaki, T. *Phys. Rev. B* **2009**, *80*, 035106.
(40) Torrance, J. B.; Shafer, M. W.; McGuire, T. R. *Phys. Rev. Lett.* **1972**, *29*, 1168.
(41) Shimakawa, Y. *Inorg. Chem.* **2008**, *47*, 8562.
(42) (a) Kobayashi, W.; Ishiwata, S.; Terasaki, I.; Takano, M.; Grigoraviciute, I.; Yamauchi, H.; Karppinen, M. *Phys. Rev. B* **2005**, *72*, 104408. (b) Sheptyakov, D. V.; Pomjakushin, V. Yu.; Drozhzhin, O. A.; Istomin, S. Ya.; Antipov, E. V.; Bobrikov, I. A.; Balagurov, A. M. *Phys. Rev. B* **2009**, *80*, 024409. (c) Fukushima, S.; Sato, T.; Akahoshi, D.; Kuwahara, H. *J. Phys. Soc. Jpn.* **2009**, *78*, 064706.
(43) Moreira dos Santos, A.; Cheetham, A. K.; Atou, T.; Syono, Y.; Yamaguchi, Y.; Ohoyama, K.; Chiba, H.; Rao, C. N. R. *Phys. Rev. B* **2002**, *66*, 064425.
(44) Hasegawa, K.; Isobe, M.; Yamauchi, T.; Ueda, H.; Yamaura, J.-I.; Gotou, H.; Yagi, T.; Sato, H.; Ueda, Y. *Phys. Rev. Lett.* **2009**, *103*, 146403.
(45) Kang, J.-S.; Lee, H. J.; Kim, D. H.; Kolesnik, S.; Dabrowski, B.; Swierczek, K.; Lee, J.; Kim, B.; Min, B. I. *Phys. Rev. B* **2009**, *80*, 045115.
(46) Gajek, M.; Bibes, M.; Barthelemy, A.; Bouzehouane, K.; Fusil, S.; Varela, M.; Fontcuberta, J.; Fert, A. *Phys. Rev. B* **2005**, *72*, 020406.